In-situ quantification of carbonate species concentrations, pH and pCO_2 in calcite fluid inclusions using confocal Raman spectroscopy.

Michael Naylor Hudgins [a,b*], Todd K. Knobbe [a], Julia Hubbard [a], Andrew Steele [c], Justin G. Park[a,b], and Morgan F. Schaller [a,b*]

[a] *Department of Earth and Environmental Sciences, Rensselaer Polytechnic Institute, Jonsson Rowland Science Center, Troy, NY, USA*

[b] *Rensselaer Astrobiology Research and Education Center, Rensselaer Polytechnic Institute, Jonsson Rowland Science Center, Troy, NY, USA*

[c] *Earth and Planets Laboratory, Carnegie Institution for Science, Washington, DC, USA*

**Corresponding Author: schall@rpi.edu*

**Co-corresponding Author: hudgim@rpi.edu*

Abstract

Carbonate minerals are globally distributed on the modern and ancient Earth and are abundant in terrestrial and marine depositional environments. Fluid inclusions hosted by calcite retain primary signatures of the source fluid geochemistry at the time of mineral formation (i.e., pCO_2) and can be used to reconstruct paleoenvironments. Confocal laser Raman spectroscopy provides a quick, non-destructive approach to measuring the constituents of fluid inclusions in carbonates and is a reliable method for determining composition in both the aqueous and gas phases in fluid inclusions. Here, we demonstrate a method for making accurate quantifications of carbonate concentrations (1.55-0.000019 molar) and pH (7-10) from fluid inclusions using confocal Raman spectroscopy. Instrument calibrations for carbonate (CO_3^{2-}) and bicarbonate (HCO_3^-) concentrations and pH were performed using stock solutions. The host mineral does not affect the carbonate species. Accurate quantification of carbonate solution concentrations and pH can be used to estimate the pCO_2 of a solution when measuring fluid inclusions with Raman spectroscopy.

Keywords: Raman spectroscopy, fluid inclusions, carbonate system, pH, CO_2, quantification

Introduction

Fluid inclusions provide a wealth of information pertaining to a mineral's environment at the time of formation[1,2]. The ability to quantify the constituents within fluid inclusions provides

information on geochemical parameters such as; initial temperature and pressure conditions, salinity, pH, and solution and gas composition of any included gas phases[3–9]. These geochemical indicators can be estimated by using Raman spectroscopy, a non-destructive method, that can be applied to the in-situ study of micron-scale fluid inclusions [6,10–14].

Calcium carbonate minerals are common and abundant in a variety of environmental settings on Earth, ranging from metamorphic carbonates forming in subduction zones[14] to low temperature authigenic marine sediments[15] and surficial deposits (pedogenic or speleothems)[16,17]. Many of these types of carbonates can contain fluid inclusions, in metamorphic carbonates they have been used to track carbon transport in Earth's interior[14] and in low-temperature carbonates fluid inclusions have been used to measure paleoenvironmental proxies in both the terrestrial and marine realms[15–18]. Many studies have focused on carbon and oxygen isotopic compositions of either the mineral matrix or fluid within inclusions[16–19], but relatively fewer studies have investigated the gas concentration or aqueous composition of fluid inclusions in non-diagenetic carbonate minerals[15,20,21].

A fundamental problem in paleoclimatology is the lack of accurate atmospheric pCO_2 estimates prior to the ice core record[22]. The proxy methods that have been deployed (e.g., the $\delta^{13}C$ of pedogenic carbonates, leaf stomatal indices, and boron isotopes[16,23–25]) show similar trends but disagree in absolute value[23–29]. However, dissolved gases and solutes in the aqueous phase of carbonate mineral fluid inclusions can provide valuable insight into the geochemical conditions of the mineral's formation environment, which can be related back to absolute atmospheric concentrations at the time of precipitation [1–4,7,30]. Unfortunately, these analyses require the destruction of fluid inclusions during bulk analyses of the released gases and require large sample sizes to enable accurate measurement[31–33]. In contrast, Raman spectroscopy is a

non-destructive method that can provide rapid analyses of liquid and gas phase compositions within individual fluid inclusions[5,34]. This method enables each of the components of the carbonate system (e.g., $[CO_3^{2-}]$, $[HCO_3^-]$, pH, and pCO_2) to be quantified discretely in-situ without disturbing the host mineral matrix. However, before quantification of any molecules measured directly within natural fluid inclusion samples, the mineral system's Raman spectrum and the host mineral's effects on solute quantification need to be evaluated.

Identification and quantification of the carbonate species (e.g., CO_3^{2-}, HCO_3^-) concentration provides information on solution pH and pCO_2 of the system that the mineral precipitated in[35]. In moderately alkaline systems, HCO_3^- is the dominant carbon species in solution, and the Raman signal of HCO_3^- has been observed in alkaline solutions in quartz hosted fluid inclusions[14,36,37]. However, these studies only recorded the presence of HCO_3^- and did not attempt to quantify the concentration. Although a weak Raman scatterer, detailed studies have shown that HCO_3^- is amenable to quantification over a range of concentrations using Raman spectroscopy[38–40]. However, these studies did not address the applicability of Raman spectroscopy to quantifying HCO_3^- concentrations in natural samples.

In this study, we present a method for the accurate measurement of $[CO_3^{2-}]$ and $[HCO_3^-]$ in fluid inclusions via Raman spectroscopy and use these measurements to estimate the pCO_2 with which the inclusion fluid had equilibrated. We construct calibration curves for CO_3^{2-} and HCO_3^- using Na_2CO_3 and $NaHCO_3$ solutions via two different methods (with and without the addition of a calcite cover slip to examine the effects of the host mineral)[41], with the ultimate goal of applying these calibrations to natural carbonate samples. We then evaluate the accuracy of each method to determine the most suitable approach for determining the concentration of CO_3^{2-} and HCO_3^- in natural fluid inclusions. We also investigate the effect of increasing solution

salinity on the quantification of solutes in fluid inclusions. These studies reveal that [CO_3^{2-}], [HCO_3^-], and the pH of alkaline solutions can be determined using the main Raman bands for CO_3^{2-} and HCO_3^-. The approaches and methods developed in this paper can be applied to a range of fluid inclusions at 1 atm. The specific effects of temperature and pressure broadening on Raman peak parameters of [CO_3^{2-}], [HCO_3^-] are not addressed in this study and has been investigated elsewhere[42,43].

Methods

Calibration Solutions

Prior Raman calibration studies for CO_3^{2-} and HCO_3^- in solution have been made at concentrations spanning from dilute solutions to near saturation ([HCO_3^-]: 1.57-0.0521 molar; [CO_3^{2-}]: 1.55-0.000019 molar)[38,44,45]. Here, we focus on calibrating the Raman response to CO_3^{2-} and HCO_3^- concentrations in dilute carbonate solutions that are closer to those observed in natural systems (Table 1). We prepared solutions of Na_2CO_3 and $NaHCO_3$ over a range of [CO_3^{2-}], [HCO_3^-], and pH that represent observed concentrations of natural systems[35,46–52] (Table 1 and 2). Natural fluid inclusions in carbonates forming at the surface and in seawater have a range of salinities[3]. Therefore, we also constructed calibrations over a range of NaCl salinities (1-5 wt%) to more closely resemble natural systems and to investigate salinity effects on the Raman peak response of carbonate species and pH quantification. We consider NaCl calibrations necessary because previous studies have demonstrated that increasing salinity alters the dissociation and solubility constants (K_{co2}, K_1, and K_2) and skews the OH^- stretch of H_2O[8,53,54], thus potentially leading to an inaccurate estimation carbonate species concentrations where freshwater calibration curves are applied to saline inclusions.

A portion of solutions were equilibrated to the atmosphere and the remainder were prepared as a close system, to encompass a full range of relevant carbonate species concentrations. Desired weights of $NaHCO_3$, Na_2CO_3, and NaCl were placed in 50 mL centrifuge tubes and continuously mixed with 50 mL of Millipore water (18 Ω) until fully dissolved. Open system solutions were mixed until equilibrium was reached. To obtain a pH <8, 1.2 molar HCl (10% HCl by volume) was added to a 0.25 molar of $NaHCO_3$ solutions. Once the acid was added, the solution was mixed until a stable pH was reached. Solution temperature and pH were measured with a Thermo Scientific Orion 2-star pH meter before measurement by Raman.

To calculate the amount of HCO_3^- and CO_3^{2-} in the closed system solutions at the time of measurement, the initial amount of HCO_3^- and CO_3^{2-} mixed in the solution was assumed to be equal to the total dissolved inorganic carbon (TDIC). Aqueous speciation of the closed carbonate system were calculated based on measured temperature and pH using the following equations[55] (Eq. 1 and 2):

$$[HCO_3^-] = C_T \frac{K_1[H^+]}{[H^+]^2 + K_1[H^+] + K_1K_2}$$

Eq. 1

$$[CO_3^{2-}] = C_T \frac{K_1K_2}{[H^+]^2 + K_1[H^+] + K_1K_2}$$

Eq. 2

Where $[HCO_3^-]$ is molar HCO_3^-; $[CO_3^{2-}]$ is molar CO_3^{2-}; C_T is molar TDIC (the initial amount of HCO_3^- and CO_3^{2-} put into solution as a $NaHCO_3$ and Na_2CO_3 salt); K_1 and K_2 are temperature-dependent equilibrium constants that account for the dissociation of H_2CO_3 and HCO_3^-, respectively; and $[H^+]$ is molar hydrogen ions.

For solutions prepared as an open system, HCO_3^- and CO_3^{2-} concentrations were calculated based on the open system equations[56]:

$$[HCO_3^-] = \frac{K_1 K_{co2} pCO_2}{[H^+]} \quad \text{Eq. 3}$$

$$[CO_3^{2-}] = \frac{K_1 K_2 K_{co2} pCO_2}{[H^+]^2} \quad \text{Eq. 4}$$

K_{CO2} (i.e., Henry's constant) is the temperature-dependent equilibrium constant that accounts for the aqueous solubility of CO_2. When estimating carbonate species concentrations for the calibrations, the equilibrium constants were adjusted to the measured temperature values using the calculations of Drever (1997)[56].

We used the closed system calculations to estimate pCO_2 in natural fluid inclusions, because the trapped solute acts as a closed system post-entrapment and the components of the fluid (alkalinity, TDIC, pH, and pCO_2) are fixed. However, the fluid inclusion would represent the environment pre-entrapment as the solute was equilibrated with the atmosphere, assuming the mineral formed at the Earth's surface. Therefore, fluid inclusions behave as a closed system and estimations of pCO_2 should use such equations.

Closed system estimations of pCO_2 require information on $[CO_3^{2-}]$, $[HCO_3^-]$, $[CO_{2\ aq}]$, and pH. Our calibrations can quantify $[CO_3^{2-}]$, $[HCO_3^-]$, and pH, but estimating $[CO_{2\ aq}]$ must be calculated because its concentration is low in the natural range chosen in this study[55] (Table 2). To estimate $[CO_{2\ aq}]$ we use the following equation:

$$[CO_{2\ aq}] = [H^+]^2 \frac{[CO_3^{2-}]}{K_1 K_2}$$

Eq. 5

Which allows for pCO_2 to be estimated from the calculated $[CO_{2\ aq}]$:

$$pCO_2 = \frac{[CO_{2\ aq}]}{K_{co2}}$$

Eq. 6

To ensure that the range of $[CO_3^{2-}]$ and $[HCO_3^-]$ captures a large range of pCO_2 values, theoretical estimations were performed using the carbonate closed system equations (Eq. 1, 2, and 5) and solved for pCO_2 (Fig. 1). These calculations show that the ratio between $[CO_3^{2-}]$ and $[HCO_3^-]$, and pH can be used to estimate a wide range of pCO_2 (-4 to 0) values (Fig. 1). The $[CO_3^{2-}]$, $[HCO_3^-]$, and pH of the Na_2CO_3 and $NaHCO_3$ solutions were input into the carbonate closed system equations to calculate the range of potential pCO_2 values. Figure 1 shows that the concentrations we selected for our solutions can be used to estimate a wide range (-4 to 0) of pCO_2.

Evaluating the Effect of the Carbonate Host Mineral

To evaluate whether the host mineral's birefringence affects the calibration curves of solute concentrations and pH in a natural carbonate sample, a cover slip was made from optical grade calcite to simulate the measurement of a calcite-hosted fluid inclusion. Previous research has demonstrated that the host mineral does not affect determination of salt concentrations in calcite when using a confocal Raman Spectrometer[8,41]. These authors suggest minimizing the effect of the host mineral in Raman spectroscopy micro-fluid inclusion studies by placing the sample at its extinction position. To test this, a piece of optical grade calcite that has the c-axis parallel to surface and free of visible inclusions and defects was used in a subset of

186 measurements to ensure the host mineral does not affect solute quantification. The cover slip was
187 ground to a thickness of ~100 microns and doubly polished to a colloidal silica grade.

188 A comparison of the standard $NaHCO_3$ and Na_2CO_3 solutions measured by Raman both
189 with and without the addition of a calcite cover slip was performed for each concentration to
190 measure the effect of the host mineral on solute quantification (Fig. 2). To ensure that the desired
191 focal plane was in the solution, before each measurement, the laser was first focused on the
192 surface of the cover slip and then focused down to the underside of the cover slip, and finally
193 focused 100 microns below and into the solution. For solutions without the calcite cover slip, the
194 laser was focused 100 microns below the surface of the solution.

195

196 *Raman Measurement and quantification of CO_3^{2-} and HCO_3^-*

197 Shortly after a solution was mixed and the open system solutions reached equilibrium, 5
198 microliters of solution were placed in a glass concavity slide and analyzed using a WiTec
199 alpha300 R confocal Raman spectrometer utilizing a 532 nm green laser at the Carnegie Institute
200 of Science, Earth and Planets Laboratory[57]. Laser power at the source was 14 mW during each
201 analysis. Measurements were made using a Zeiss 50x objective, a 50 μm aperture, and a 1 cm^{-1}
202 spectral resolution using a Witec UHTS spectrometer system with a 600 grating and an Andor
203 DV400 camera cooled to -59 °C. Additional measurements were made on a Bruker SENTERRA
204 Raman spectrometer at Rensselaer Polytechnic Institute, Department of Earth and Environmental
205 Science. Measurements were integrated for 30 seconds with 3 accumulations and alternated
206 between the solution and the solution with calcite cover slip to minimize any evolution in the
207 solution composition over the course of the analyses. Each component (H_2O, HCO_3^-, and CO_3^{2-}
208 solution with and without the calcite cover slip, and the calcite cover slip alone) used in this

study can be broken down into their individual Raman spectra (i.e., H_2O, $CaCO_3$, etc. measured independently), and when constructed together, form a spectra that simulates a fluid inclusion (Fig.2).

The HCO_3^- anion has a weak Raman scatter, but in alkaline solutions, HCO_3^- is the dominant anion of the carbonate system and has 9 normal, partially polarized Raman modes [5,40,58]. The two broad, weak peaks at 634 cm^{-1} and 673 cm^{-1} with the latter representing δCO2. The broad mode at 634 cm^{-1} can be deconvoluted into three sub-bands at 630 cm^{-1}, 634 cm^{-1}, and 640 cm^{-1} to represent γCO-H and δHOC. HCO_3^- modes are prevalent at 843 cm^{-1} (γCO_3), 1017 cm^{-1} (νC-OH), 1312 cm^{-1} (δCO-H), 1360 cm^{-1} ($\nu_s CO_2$), 1630 cm^{-1} ($\nu_{as} CO_2$), and 2600 cm^{-1} (νCO-H)[40]. The Raman bands of CO_3^{2-} have 6 active Raman modes[5,38], where weak peaks occur at 684 cm^{-1} (ν_4, in-plane deformation), 885 cm^{-1} (ν_2, out-of-plane deformation), 1385 cm^{-1} (ν_3, antisymmetric stretch C-O), 1435 cm^{-1}, and 1764 cm^{-1}[40]. However, to avoid issues with peak interferences, low intensity signals, and/or mineral fluorescence, the main vibrational mode of HCO_3^- at 1017 cm^{-1} and CO_3^{2-} at 1066 cm^{-1} was used to quantify the amount of [HCO_3^-] and [CO_3^{2-}] in solutions as these are the strongest peaks[5,40]. Calibration solution data was exported in OriginLab (OriginLab Corp., Northampton, MA, USA) where the spectra was background subtracted and the main HCO_3^- and CO_3^{2-} bands were integrated for their cumulative area (A_{HCO-3-} and A_{CO32-}). The area of the HCO_3^- and CO_3^{2-} bands were ratioed (A_{CO32-}/A_{HCO3-}) as this parameter is reliable in estimating pH, as well as [CO_3^{2-}], and [HCO_3^-] as the concentrations are pH dependent (Fig. 1). The ratioed area of the bands, the measured pH, and the calculated [HCO_3^-] and [CO_3^{2-}] of calibration solutions are used to build calibration curves which allows us to estimate [CO_3^{2-}], [HCO_3^-], and pH of an unknown sample[38,59].

Optical Calcite Fluid Inclusion

An Icelandic Spar calcite sample of an unknown origin was used to evaluate the applicability of our calibration's curves to natural carbonate samples. The Icelandic Spar calcite was chosen as a test sample, as it contained an abundance of primary and secondary fluid inclusions spanning a large size range. An inclusion-free portion of the same mineral was used to make the calcite cover slip and provides the best matrix matched sample to test the calibration curves. The fluid inclusions in the Icelandic Spar calcite are predominantly of two phases, vapor and liquid. For demonstration of the success of the calibration technique, a large inclusion that is ~150 μm across and ~150 μm below the sample surface was analyzed. Measurements were focused on a large ~150 μm fluid inclusion because the area of the phases (aqueous or vapor) of interest were larger than the laser spot size (~1 μm or less). Fluorescence from the host calcite makes it increasingly difficult to analyze small inclusions, especially as parameters such as integration time and accumulations are increased. If carbonate species concentrations and pH of the solution are quantified, then the pCO_2 can be determined in a fluid inclusion using equation six[55]. The spectra of the Icelandic Spar calcite were processed and deconvoluted as the calibration solution, as described in the previous section.

Results and Discussion

Calibration Curves

Aqueous bicarbonate and carbonate calibration curves were made for a range of solution to calibrate the Raman spectrometer to quantify carbonate species concentrations and pH and to investigate the effects of the host mineral and salinity on carbonate species and pH quantification.

Area ratio calibrations for standard solutions (without NaCl) with and without the calcite cover slip are similar (Fig. 3 and Table 3; consult this table for equations). Quantification of $[CO_3^{2-}]$, $[HCO_3^-]$, and pH using A_{CO32-}/A_{HCO3-} show a power, linear, and exponential relationship, respectively, with and without the calcite cover slip (Fig. 3). NaCl wt% calibration curves display a spreading pattern for $[CO_3^{2-}]$ and pH estimations with increasing salinity, whereas $[HCO_3^-]$ have similar slopes and intercepts (Fig. 4 and Table 4; consult this table for equations). Quantification of $[CO_3^{2-}]$, $[HCO_3^-]$, and pH using A_{CO32-}/A_{HCO3-} with increasing salinity shows a power, linear, and exponential relationship, respectively.

Characterization of the Raman spectra

The solutions with the calcite cover slip have a peak at 1088 cm^{-1} that may interfere with CO_3^{2-} in solution and can pose a potential problem in accurately quantifying carbonate species at low concentrations in fluid inclusions, as discussed in Dubessy et al. (1992)[12]. However, the confocal Raman spectrometer also detects a low $CaCO_3$ peak at 1088 cm^{-1} that does not interfere with the CO_3^{2-} signal (Fig. 2). With this, the calcite cover slip has little to no effect on estimating $[CO_3^{2-}]$, $[HCO_3^-]$, and pH of the system when using area ratio between the carbonate species. At lower concentrations, HCO_3^- and CO_3^{2-} becomes harder to distinguish from the background (pH = <7) and perhaps an additional extrapolation scheme may be needed.

Caumon et al. (2015)[41] demonstrated that if the crystal symmetry and optical properties are not accounted for then quantification errors can occur. However, this is not a concern in our analyses because we employ a confocal Raman spectrometer which bypasses the calcite cover slip as it is above the focal point and does not contribute to the analysis[34,60]. Given this, there is no substantial difference expected, and accordingly little effect is observed on the calibration curves between non- and calcite cover slip analyses (Fig. 3). The confidence intervals indicate no

major differences between non-calcite cover slip and calcite cover slip as they overlap one another (Table 3).

The effects of salinity on the calibrations at low [CO_3^{2-}] and pH is likely negligible ([CO_3^{2-}] <0.01 molar and ~9.5 pH) (Fig. 4). However, accounting for salinity in estimating [HCO_3^-] is likely minor at all concentrations as the slope of the calibrations for different salinities overlap within their respective confidence intervals (Fig. 4 and Table 4). Therefore, it may be unnecessary to account for the effects of salinity for a solution at low concentrations (e.g., seawater) and pH in natural fluid inclusions. Although, at higher [CO_3^{2-}] and pH, salinity should be considered by using the OH^- Raman stretch to quantify the concentration of NaCl[6,8]. Their methods to determine NaCl concentration can be applied to natural fluid inclusions to allow for accurate [CO_3^{2-}], [HCO_3^-], and pH estimates using our calibrations. Overall, the relationships observed are a promising approach towards accurately quantifying carbonate species and pH to estimate pCO_2 in natural samples.

Measurement of fluid inclusion in Calcite

The results of measurements of the aqueous and gaseous phases of a ~150 microns fluid inclusion in the Icelandic Spar calcite are shown in Figure 5. The inclusion formed in an area of the crystal that showed no signs of fracture healing or continual mineral growth along a growth plane[61]. Because the origin, internal pressure, density, and temperature of formation of the fluid inclusion is unknown, this section and the measurements described within are presented as a demonstrative proof of concept. We chose this sample for its ample size. Given this, the density of the gaseous phase CO_2 can be determined by using the Fermi diad peak difference (ν_1-$2\nu_2$) of CO_2[62,63]. It is worth noting that although fluid inclusion homogenization experiments can be used to determine temperature of formation, it is beyond the scope of this study.

In the aqueous phase spectra, the distinctive peaks of the calcite host mineral can be observed as well as a HCO_3^- and CO_3^{2-}peak at 1017 cm^{-1} and 1066 cm^{-1}, respectively (Fig. 5). The OH^- stretch is present between 2750-3700 cm^{-1}. The salinity in the fluid inclusion was estimated to be 19.9 wt% using the equation of Wang et al. (2013), assuming that NaCl only is present in solution[64]. The area between the HCO_3^- and CO_3^{2-} peaks were calculated, ratioed, and applied to the calibration curves without the calcite cover slip. pH was estimated to be 9.46 ± 0.31, and [HCO_3^-] and [CO_3^{2-}] were determined to be 0.04 ± 0.02 and 0.05 ± 0.08 molar, respectively (Table 5). The dissociation and solubility constants were adjusted to the measured salinity value using the calculations of Millero (2006)[53] and Onda et al. (1970)[54]. 20C° was assumed for the solubility and dissociation constants to calculate pCO_2 because the temperature at the time of formation is unknown. With carbonate concentrations and solution pH estimated, $pCO_{2(g)}$ was calculated to be -3.62 ± 0.19 (240 ± 132 ppm).

In the gaseous phase spectra, the CO_2 Fermi diad is present at 1287 cm^{-1} and 1389 cm^{-1}, hydrogen sulfide and methane are also present at 2611 cm^{-1} and 2917 cm^{-1}, respectively[5] (Fig. 5). The density of CO_2 is essentially zero as the fermi diad technique can be utilized as low as 0.1 g/cm^3[62,63]. However, the density of present-day atmospheric CO_2 is 0.0019 g/cm^3, potentially suggesting that the fluid inclusion formed in an atmosphere between <0.0019 and <0.1 g/cm^3 of CO_2. In addition, the lack of major atmospheric gases (e.g., O_2 and N_2), the presence of H_2S and CH_4 suggest that the fluid inclusion precipitated in a reducing environment.

Calibration Limitations

Quantification of [CO_3^{2-}], [HCO_3^-], and pH can provide information about the pCO_2 of formation of a carbonate fluid inclusion, and there is no observed effect from the host mineral on

estimating pH and carbonate species when using a confocal instrument (Fig. 3)[8,41]. However, there are limitations using this method, including: (1) the Raman spectrometer was calibrated at low temperatures and pressures (1 atm), where it is likely the calibrations will deviate at higher temperatures and pressures as the solubilities and the dissociation constants of the carbonate species change[65,66]. (2) The calibrated Raman spectrometer does not encompass the low pH range present in modern [48,52] and ancient systems[46] (e.g., acidic springs and soils). (3) Determining the alkalinity of fluid inclusions may be impossible with current technology as titrating them would lead to fluid contamination. However, it is reasonable to assume that the alkalinity would be controlled by TDIC, as it is in the modern oceans[67]. (4) Salts (e.g., $MgCl_2$, $CaCl_2$, and KCl) are likely to be present in natural carbonate fluid inclusions that will skew the water peaks[8,64] and may affect accurate determination of pH and species concentrations. (5) Analyses of fluid inclusions are based on small amounts of solution, and this limits the determination of carbonate species concentrations and pH, as a relationship exists between the intensity and the number of molecules present in the sample[68]. For example, if there is a limited amount of water in a carbonate fluid inclusion, a lower intensity water peak will be observed, and as a consequence of this, the HCO_3^- and CO_3^{2-} peaks may not be detectable in these inclusions. However, larger carbonate fluid inclusions are promising as more solution is present and may be able to detect HCO_3^- and CO_3^{2-} (Fig. 5).

Other Applications

The different proxies to estimate pCO_2 in deep time do not agree with one another[16,23–25]. For example, data from $\delta^{13}C$ of paleosol carbonates and stomatal indices of fossil plants from the end-Triassic extinction show a corroborating pCO_2 trend, but the absolute pCO_2 values do not agree[26–28]. One reason is the soil productivity parameter (S(z)) within the soil diffusion model[25].

This parameter is the concentration of CO_2 in the soil derived from the respiration of organic matter and CO_2 in the atmosphere. CO_2 estimations within a soil is largely unknown and unconstrained because this parameter will fluctuate depending on soil profile depth and soil type[16]. However, the calibration presented in this study is a potential method that can constrain the S(z) and estimate pCO_2 within a soil column.

Conclusion

We demonstrate the calibration of a confocal Raman spectrometer over a range of [CO_3^{2-}], [HCO_3^-], and pH, representative of natural waters. These calibrations allow for the quantification of carbonate species concentrations and pH in fluid inclusion at low-temperatures and pressures. Calibrations can be used to calculate [CO_3^{2-}], [HCO_3^-], and pH, which ultimately allows pCO_2 to be determined in mineral fluid inclusions, assuming the mineral formed at the Earth's surface and equilibrated with its environment. The host mineral's crystal optics have little to no effect on determining the [CO_3^{2-}], [HCO_3^-], and pH if the Raman spectrometer is confocal. Negligeable effects of salinity occur at low [CO_3^{2-}] and pH, and all [HCO_3^-]. Homogenization temperature experiments should be conducted in conjunction with confocal Raman experiments to determine accurate pCO_2 estimations in natural fluid inclusions.

Acknowledgements

This research was supported by NASA Earth First Origins grant A129942527. We would like to thank Oliver Wolfe, Samantha Pyror, Nikos Sitaras, Sebastian Barkett, Mikayla Berman, Kristin Johnson-Finn, Jacob Shelley, Frank Spear, and Kristen Chiama for enlightening discussions, edits, and feedback that greatly improved this manuscript. The authors thank the anonymous reviewers for their valuable feedback, and suggestions that greatly improved the quality of the manuscript.

Declaration of Conflicting Interest

The authors declare that there is no conflict of interest.

References

1. R.H. Goldstein. “Clues from Fluid Inclusions”. Science. American Association for the Advancement of Science, 2001. 294(5544): 1009–1011. 10.1126/science.1066322.
2. E. Roedder. “Introduction to Fluid Inclusions”. Mineralogical Society of America. 1984. 12: 1–10.
3. R.J. Bodnar. Chapter 4. Introduction to Aqueous-Electrolyte Fluid Inclusions. Mineral. Assoc. Canada, 2003.
4. L.W. Diamond. Chapter 3. Systematics of H2O Inclusions. Mineral. Assoc. Canada, 2003.
5. M.L. Frezzotti, F. Tecce, A. Casagli. “Raman spectroscopy for fluid inclusion analysis”. Journal of Geochemical Exploration. 2012. 112: 1–20. 10.1016/j.gexplo.2011.09.009.
6. T.P. Mernagh, A.R. Wilde. “The use of the laser Raman microprobe for the determination of salinity in fluid inclusions”. Geochimica et Cosmochimica Acta. 1989. 53(4): 765–771. 10.1016/0016-7037(89)90022-7.
7. T.K. Lowenstein, M.N. Timofeeff, S.T. Brennan, L.A. Hardie, R.V. Demicco. “Oscillations in Phanerozoic Seawater Chemistry: Evidence from Fluid Inclusions”. Science. American Association for the Advancement of Science, 2001. 294(5544): 1086–1088. 10.1126/science.1064280.
8. Q. Sun, L. Zhao, N. Li, J. Liu. “Raman spectroscopic study for the determination of Cl− concentration (molarity scale) in aqueous solutions: Application to fluid inclusions”. Chemical Geology. 2010. 272(1–4): 55–61. 10.1016/j.chemgeo.2010.02.004.
9. T. Azbej, M.J. Severs, B.G. Rusk, R.J. Bodnar. “In situ quantitative analysis of individual H2O–CO2 fluid inclusions by laser Raman spectroscopy”. Chemical Geology. 2007. 237(3–4): 255–263. 10.1016/j.chemgeo.2006.06.025.
10. Brigitte. Wopenka, J.Dill. Pasteris. “Raman intensities and detection limits of geochemically relevant gas mixtures for a laser Raman microprobe”. Anal. Chem. 1987. 59(17): 2165–2170. 10.1021/ac00144a034.
11. J. Dubessy, B. Poty, C. Ramboz. “Advances in C-O-H-N-S fluid geochemistry based on micro-Raman spectrometric analysis of fluid inclusions”. European Journal of Mineralogy. 1989. 1(4): 517–534.
12. J. Dubessy, M.-C. Boiron, A. Moissette, C. Monnin, N. Sretenskaya. “Determination of water, hydrates and pH in fluid inclusions by micro-Raman spectrometry”. European Journal of Mineralogy. 1992. 4: 885–894. 10.1127/ejm/4/5/0885.
13. E.A.J. Burke. “Raman microspectrometry of fluid inclusions”. Lithos. 2001. 55(1): 139–158. 10.1016/S0024-4937(00)00043-8.

14. M.L. Frezzotti, J. Selverstone, Z.D. Sharp, R. Compagnoni. “Carbonate dissolution during subduction revealed by diamond-bearing rocks from the Alps”. Nature Geosci. Nature Publishing Group, 2011. 4(10): 703–706. 10.1038/ngeo1246.

15. U. Brand, N. Blamey, C. Garbelli, E. Griesshaber, R. Posenato, L. Angiolini, et al. “Methane Hydrate: Killer cause of Earth’s greatest mass extinction”. Palaeoworld. 2016. 25(4): 496–507. 10.1016/j.palwor.2016.06.002.

16. T.E. Cerling. “Stable Carbon Isotopes in Palaeosol Carbonates”. In: M. Thiry, R. Simon-Coinçon, editors. Palaeoweathering, Palaeosurfaces and Related Continental Deposits. Blackwell Publishing Ltd., Oxford, UK, 2009. Pp. 43–60. 10.1002/9781444304190.ch2.

17. M.L. Griffiths, R.N. Drysdale, H.B. Vonhof, M.K. Gagan, J. Zhao, L.K. Ayliffe, et al. “Younger Dryas–Holocene temperature and rainfall history of southern Indonesia from δ18O in speleothem calcite and fluid inclusions”. Earth and Planetary Science Letters. 2010. 295(1): 30–36. 10.1016/j.epsl.2010.03.018.

18. N. Tabor, T. Myers. “Paleosols as Indicators of Paleoenvironment and Paleoclimate”. Annual Review of Earth and Planetary Sciences. 2014. 43: 150317182938004. 10.1146/annurev-earth-060614-105355.

19. H.P. Schwarcz, R.S. Harmon, P. Thompson, D.C. Ford. “Stable isotope studies of fluid inclusions in speleothems and their paleoclimatic significance”. Geochimica et Cosmochimica Acta. 1976. 40(6): 657–665. 10.1016/0016-7037(76)90111-3.

20. K. Azmy, N.J.F. Blamey. “Source of diagenetic fluids from fluid-inclusion gas ratios”. Chemical Geology. 2013. 347: 246–254. 10.1016/j.chemgeo.2013.04.011.

21. N. Blamey, N.M.I. of Mining, P. Boston, L. Rosales-Lagarde, N.M.I. of Mining, N.S. College. “High-resolution signatures of oxygenation and microbiological activity in speleothem fluid inclusions”. International Journal of Speleology. 2016. 45(3): 231–241.

22. D. Lüthi, M. Le Floch, B. Bereiter, T. Blunier, J.-M. Barnola, U. Siegenthaler, et al. “High-resolution carbon dioxide concentration record 650,000–800,000 years before present”. Nature. 2008. 453(7193): 379–382. 10.1038/nature06949.

23. D.L. Royer, K.M. Moynihan, M.L. McKee, L. Londoño, P.J. Franks. “Sensitivity of a leaf gas-exchange model for estimating paleoatmospheric CO_2 concentration”. Climate of the Past. Copernicus GmbH, 2019. 15(2): 795–809. 10.5194/cp-15-795-2019.

24. S.M. Eggins, L.L. Haynes, K.A. Allen, K.D. Holland, K. Lorbacher, B. Hönisch. Boron Proxies in Paleoceanography and Paleoclimatology. 1st edition. Wiley-Blackwell, Hoboken, NJ, 2019.

25. D.O. Breecker. “Quantifying and understanding the uncertainty of atmospheric CO2 concentrations determined from calcic paleosols”. Geochemistry, Geophysics, Geosystems. 2013. 14(8): 3210–3220. 10.1002/ggge.20189.

26. M.F. Schaller, J.D. Wright, D.V. Kent. “Atmospheric Pco2 Perturbations Associated with the Central Atlantic Magmatic Province”. Science. 2011. 331(6023): 1404–1409. 10.1126/science.1199011.

27. M.F. Schaller, J.D. Wright, D.V. Kent, P.E. Olsen. “Rapid emplacement of the Central Atlantic Magmatic Province as a net sink for CO2”. Earth and Planetary Science Letters. 2012. 323–324: 27–39. 10.7916/D8PG22B4.

28. J.C. McElwain, D.J. Beerling, F.I. Woodward. “Fossil Plants and Global Warming at the Triassic-Jurassic Boundary”. Science. 1999. 285(5432): 1386–1390. 10.1126/science.285.5432.1386.

29. T.E. Cerling. “Stable Carbon Isotopes in Palaeosol Carbonates”. Palaeoweathering, Palaeosurfaces and Related Continental Deposits. Wiley-Blackwell, 2009. Pp. 43–60.

30. L.W. Diamond. “Review of the systematics of CO2–H2O fluid inclusions”. Lithos. 2001. 55(1–4): 69–99. 10.1016/S0024-4937(00)00039-6.

31. J.L. Zimmermann, R. Moretto. “Release of water and gases from halite crystals”. European Journal of Mineralogy. 1996. 8(2): 413–422.

32. D.I. Norman, N. Blamey, J.N. Moore. “INTERPRETING GEOTHERMAL PROCESSES AND FLUID SOURCES FROM FLUID INCLUSION ORGANIC COMPOUNDS AND CO2/N2 RATIOS”. Twenty-Seventh Workshop on Geothermal Reservoir Engineering. 2002.

33. A.E. Williams. “Mass spectrometric analysis of volatiles in fluid inclusions: aliquot calibration valve to simulate inclusion rupture”. Chemical Geology. 1996. 131(1): 155–165. 10.1016/0009-2541(96)00064-2.

34. M. Fries, A. Steele. “Raman Spectroscopy and Confocal Raman Imaging in Mineralogy and Petrography”. Springer Series in Optical Sciences. 2011. Pp. 111–135. 10.1007/978-3-642-12522-5_6.

35. J.N. Butler. Carbon Dioxide Equilibria and their Applications. Routledge, New York, 1982. 10.1201/9781315138770.

36. T. Hrstka, J. Dubessy, J. Zachariáš. “Bicarbonate-rich fluid inclusions and hydrogen diffusion in quartz from the Libčice orogenic gold deposit, Bohemian Massif”. Chemical Geology. 2011. 281(3–4): 317–332. 10.1016/j.chemgeo.2010.12.018.

37. S. Facq, I. Daniel, G. Montagnac, H. Cardon, D.A. Sverjensky. “In situ Raman study and thermodynamic model of aqueous carbonate speciation in equilibrium with aragonite under subduction zone conditions”. Geochimica et Cosmochimica Acta. 2014. 132: 375–390. 10.1016/j.gca.2014.01.030.

38. B.G. Oliver, A.R. Davis. “Vibrational Spectroscopic Studies of Aqueous Alkali Metal Bicarbonate and Carbonate Solutions”. Can. J. Chem. 1973. 51(5): 698–702. 10.1139/v73-106.

39. W.W. Rudolph, D. Fischer, G. Irmer. “Vibrational Spectroscopic Studies and Density Functional Theory Calculations of Speciation in the CO_2—Water System”. Appl Spectrosc. 2006. 60(2): 130–144. 10.1366/000370206776023421.

40. W.W. Rudolph, G. Irmer, E. Königsberger. “Speciation studies in aqueous HCO3−–CO32− solutions. A combined Raman spectroscopic and thermodynamic study”. Dalton Trans. The Royal Society of Chemistry, 2008. (7): 900–908. 10.1039/B713254A.

41. M.-C. Caumon, A. Tarantola, R. Mosser-Ruck. “Raman spectra of water in fluid inclusions: I. Effect of host mineral birefringence on salinity measurement”. Journal of Raman Spectroscopy. 2015. 46(10): 969–976. 10.1002/jrs.4708.

42. J.D. Frantz. “Raman spectra of potassium carbonate and bicarbonate aqueous fluids at elevated temperatures and pressures: comparison with theoretical simulations”. Chemical Geology. 1998. 152(3): 211–225.

43. J. Wu, H. Zheng. “Quantitative measurement of the concentration of sodium carbonate in the system of Na2CO3–H2O by Raman spectroscopy”. Chemical Geology. 2010. 273(3): 267–271. 10.1016/j.chemgeo.2010.03.001.

44. W.W. Rudolph, G. Irmer, E. Königsberger. “Speciation studies in aqueous HCO3−–CO32− solutions. A combined Raman spectroscopic and thermodynamic study”. Dalton Trans. The Royal Society of Chemistry, 2008. (7): 900–908. 10.1039/B713254A.

45. Q. Sun, C. Qin. “Raman OH stretching band of water as an internal standard to determine carbonate concentrations”. Chemical Geology. 2011. 283(3): 274–278. 10.1016/j.chemgeo.2011.01.025.

46. K.E. Chave. “Evidence on History of Sea Water from Chemistry of Deeper Subsurface Waters of Ancient Basins1”. AAPG Bulletin. 1960. 44(3): 357–370. 10.1306/0BDA5FF3-16BD-11D7-8645000102C1865D.

47. F.T. Mackenzie, R.M. Garrels. “Chemical mass balance between rivers and oceans”. American Journal of Science. American Journal of Science, 1966. 264(7): 507–525. 10.2475/ajs.264.7.507.

48. R.M. Garrels, F. Mackenzie. “Origin of the Chemical Compositions of Some Springs and Lakes”. Am. Chem. Soc. Adv. Chem. Ser. 1967. Pp. 222–242. 10.1021/ba-1967-0067.ch010.

49. S.D. Burley, J. Mullis, A. Matter. “Timing diagenesis in the Tartan Reservoir (UK North Sea): constraints from combined cathodoluminescence microscopy and fluid inclusion studies”. Marine and Petroleum Geology. 1989. 6(2): 98–120. 10.1016/0264-8172(89)90014-7.

50. W. Stumm, J.J. Morgan. Aquatic Chemistry: Chemical Equilibria and Rates in Natural Waters. Wiley, 1996.

51. D. Langmuir. Aqueous Environmental Geochemistry. 1st edition. Prentice Hall, Upper Saddle River, N.J, 1997.

52. M.E. Sumner, ed. Handbook of Soil Science. 1st edition. CRC Press, Boca Raton, Fla, 1999.

53. F.J. Millero, T.B. Graham, F. Huang, H. Bustos-Serrano, D. Pierrot. “Dissociation constants of carbonic acid in seawater as a function of salinity and temperature”. Marine Chemistry. 2006. 100(1): 80–94. 10.1016/j.marchem.2005.12.001.

54. K. Onda, E. Sada, T. Kobayashi, S. Kito, K. Ito. “SALTING-OUT PARAMETERS OF GAS SOLUBILITY IN AQUEOUS SALT SOLUTIONS”. J. Chem. Eng. Japan / JCEJ. 1970. 3(1): 18–24. 10.1252/jcej.3.18.

55. J.N. Butler. Ionic Equilibrium: Solubility and pH Calculations. John Wiley & Sons, 1998.

56. J.I. Drever. The Geochemistry of Natural Waters: Surface and Groundwater Environments. Prentice Hall, 1997.

57. T. Dieing, O. Hollricher. “High-resolution, high-speed confocal Raman imaging”. Vibrational Spectroscopy. 2008. 48(1): 22–27. 10.1016/j.vibspec.2008.03.004.

58. A.R. Davis, B.G. Oliver. “A Vibrational-Spectroscopic Study of the Species Present in the CO2-HzO System”. Journal of Solution Chemistry. 1972. 1(4): 11.

59. J.D. Pasteris, O. Beyssac. “Welcome to Raman Spectroscopy: Successes, Challenges, and Pitfalls”. Elements. 2020. 16(2): 87–92. 10.2138/gselements.16.2.87.

60. G. Giridhar, R.R.K.N. Manepalli, G. Apparao. “Confocal Raman Spectroscopy”. Spectroscopic Methods for Nanomaterials Characterization. Elsevier, 2017. Pp. 141–161. 10.1016/B978-0-323-46140-5.00007-8.

61. R.H. Goldstein. Chapter 2: Petrographic Analysis of Fluid Inclusions. Mineral. Assoc. Canada, 2003.

62. K.M. Rosso, R.J. Bodnar. “Microthermometric and Raman spectroscopic detection limits of C02 in fluid inclusions and the Raman spectroscopic characterization of C02”. Geochimica et Cosmochimica Acta. 1995. 59(19): 3961–3975. 10.1016/0016-7037(95)94441-H.

63. Y. Kawakami, J. Yamamoto, H. Kagi. “Micro-Raman Densimeter for CO_2 Inclusions in Mantle-Derived Minerals”. Appl Spectrosc. 2003. 57(11): 1333–1339. 10.1366/000370203322554473.

64. X. Wang, W. Hu, I.-M. Chou. “Raman spectroscopic characterization on the OH stretching bands in NaCl–Na2CO3–Na2SO4–CO2–H2O systems: Implications for the measurement of chloride concentrations in fluid inclusions”. Journal of Geochemical Exploration. 2013. 132: 111–119. 10.1016/j.gexplo.2013.06.006.

65. J.J. Carroll, J.D. Slupsky, A.E. Mather. “The Solubility of Carbon Dioxide in Water at Low Pressure”. Journal of Physical and Chemical Reference Data. American Institute of Physics, 1991. 20(6): 1201–1209. 10.1063/1.555900.

66. R. Wiebe, V.L. Gaddy. “The Solubility of Carbon Dioxide in Water at Various Temperatures from 12 to 40° and at Pressures to 500 Atmospheres. Critical Phenomena *”. J. Am. Chem. Soc. 1940. 62(4): 815–817. 10.1021/ja01861a033.

67. R.E. Zeebe, D. Wolf-Gladrow. CO2 in Seawater: Equilibrium, Kinetics, Isotopes. Gulf Professional Publishing, 2001.

68. M.J. Pelletier. Analytical Applications of Raman Spectroscopy. 1st edition. Blackwell Publishing, Osney Mead, Oxford ; Malden, MA, 1999.

69. J.A. Hurowitz, D.C. Catling, W.W. Fischer. “High Carbonate Alkalinity Lakes on Mars and their Potential Role in an Origin of Life Beyond Earth”. Elements. 2023. 19(1): 37–44. 10.2138/gselements.19.1.37.

Figures and Tables

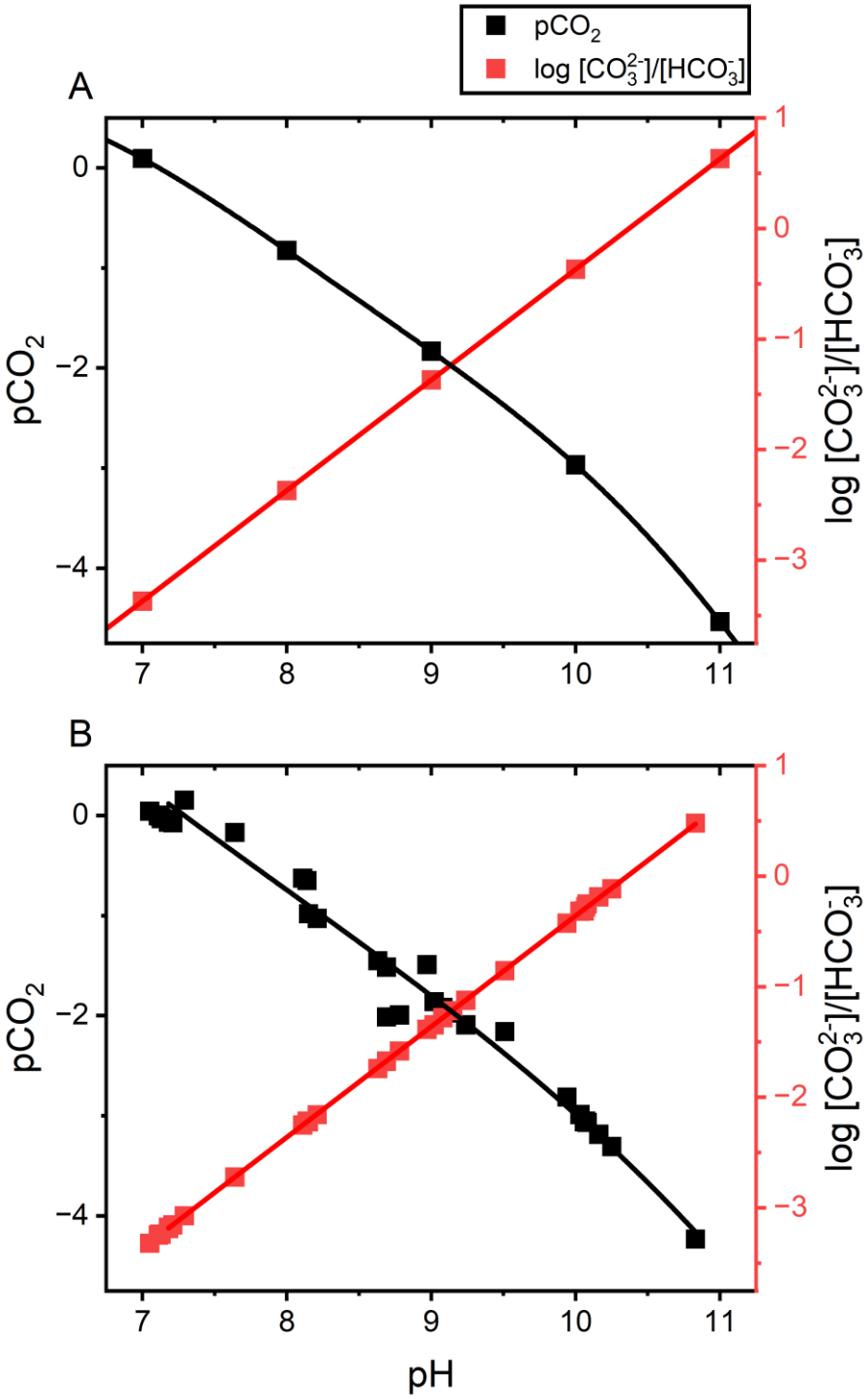

Figure 1. (A) Theoretical calculations of the relationship between the ratio of $[CO_3^{2-}]$ and $[HCO_3^-]$, pH, and pCO_2. The theoretical relationship can be used to estimate pCO_2 over a wide range of alkaline solutions. (B) Solutions used in this study shows the relationship between the ratio of $[CO_3^{2-}]$ and $[HCO_3^-]$, and pH can calibrate for a wide range of pCO_2.

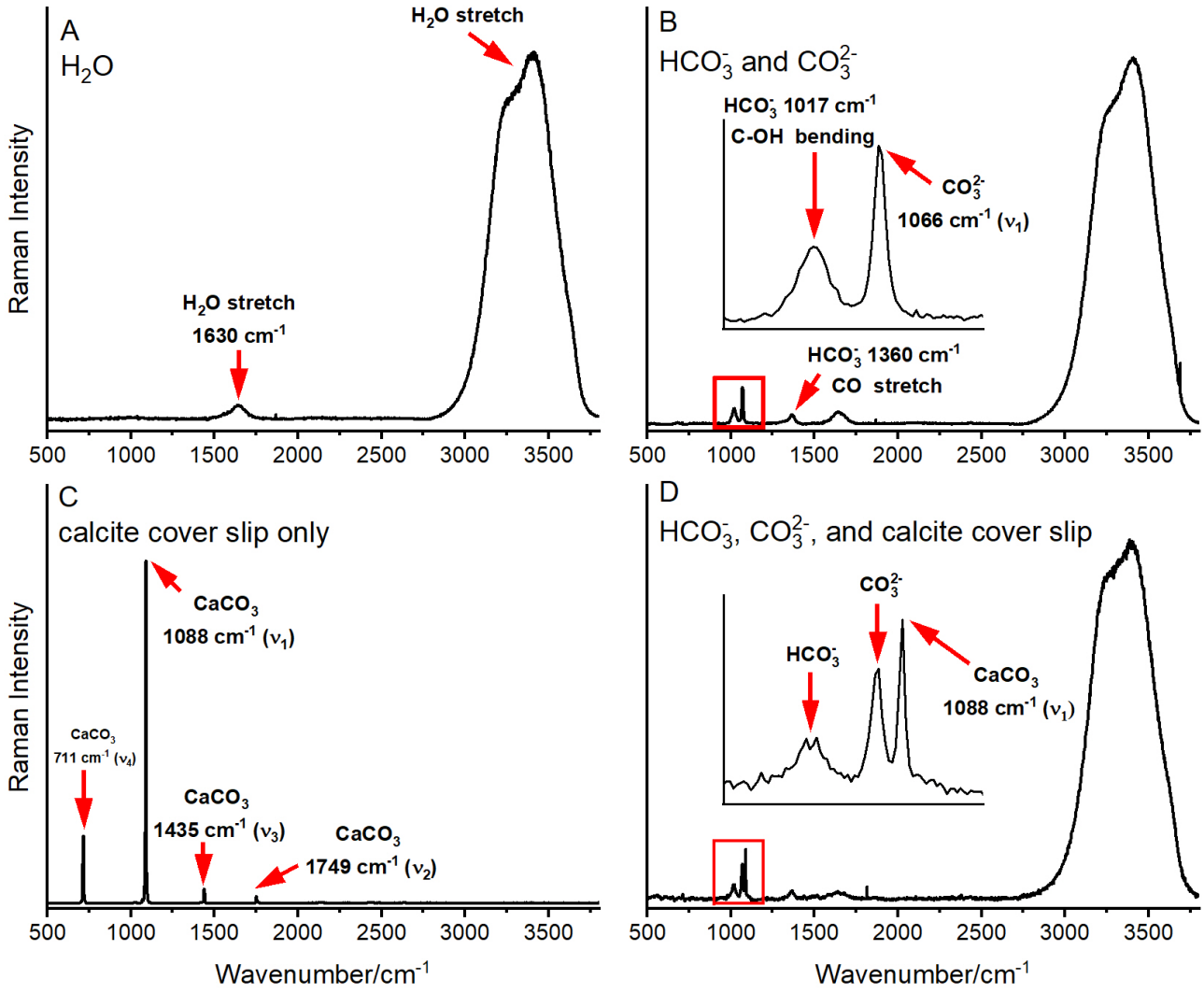

Figure 2. Background corrected Raman spectra of the different components used to build the calibration curves. A) Raman spectra of the Millipore water used to make the solutions. B) Raman spectra of a 0.15 molar $NaHCO_3$ and 0.03 molar Na_2CO_3 solution with inset of the red box in an area between 950 – 1150 cm^{-1}. The main HCO_3^- and CO_3^{2-} band is at ~1017 and ~1066 cm^{-1}, respectively. C) Raman spectra of the calcite cover slip with the main $CaCO_3$ peak at ~1088 cm^{-1}. D) Raman spectra of the 0.15 molar $NaHCO_3$ and 0.03 molar Na_2CO_3 solution with the Raman focused 100 µm below the calcite cover slip with an inset that shows the respective positions of the HCO_3^-, CO_3^{2-}, and $CaCO_3$ peaks. Abbreviations: T, translational lattice; ν_1, symmetric stretching vibration; ν_2, out-of-plane bending vibration; ν_3, antisymmetric stretching vibration; ν_4, in-plane bending vibration.

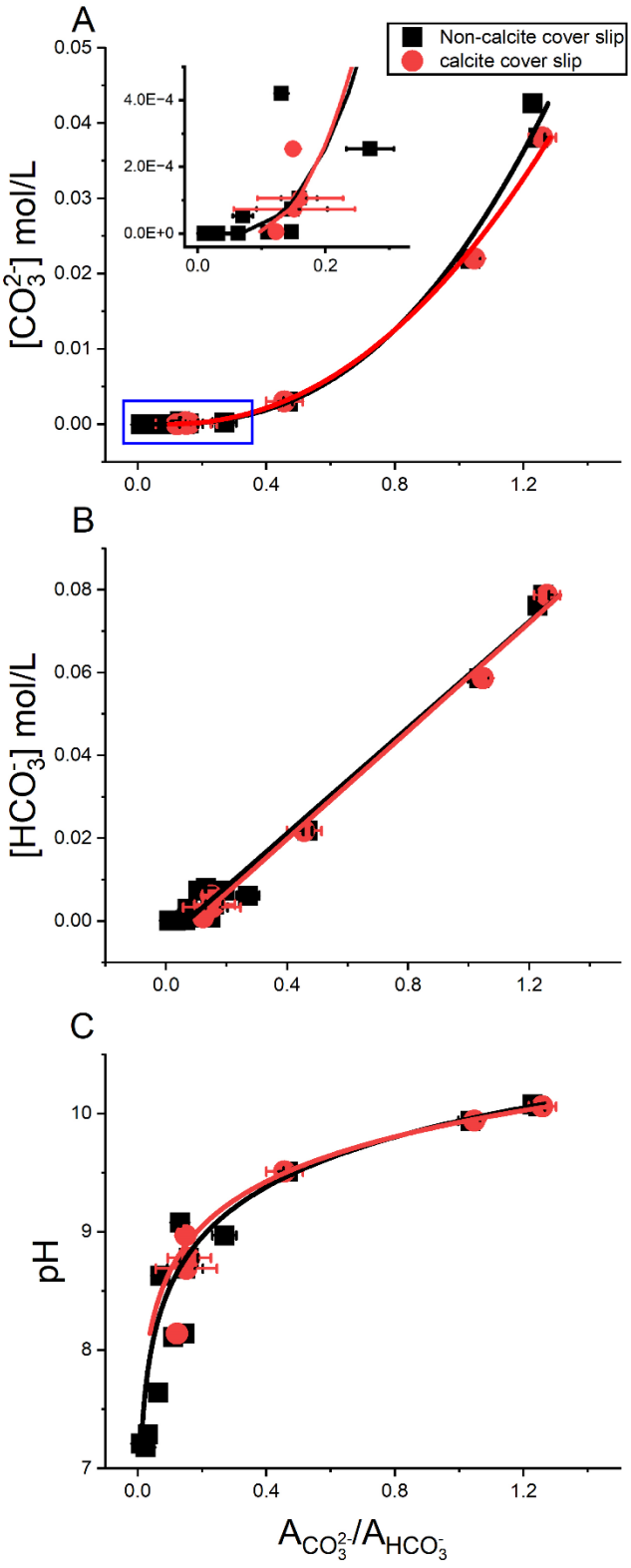

Figure 3. Comparisons of carbonate species concentrations and pH solution calibrations with (red) and without (black) the calcite cover slip. Solution calibrations of $[CO_3^{2-}]$ (A), $[HCO_3^-]$ (B), and pH (C) versus the area ratio between CO_3^{2-} and HCO_3^- peaks. Blue box represents the inset within (A). Concentrations are in mol/L.

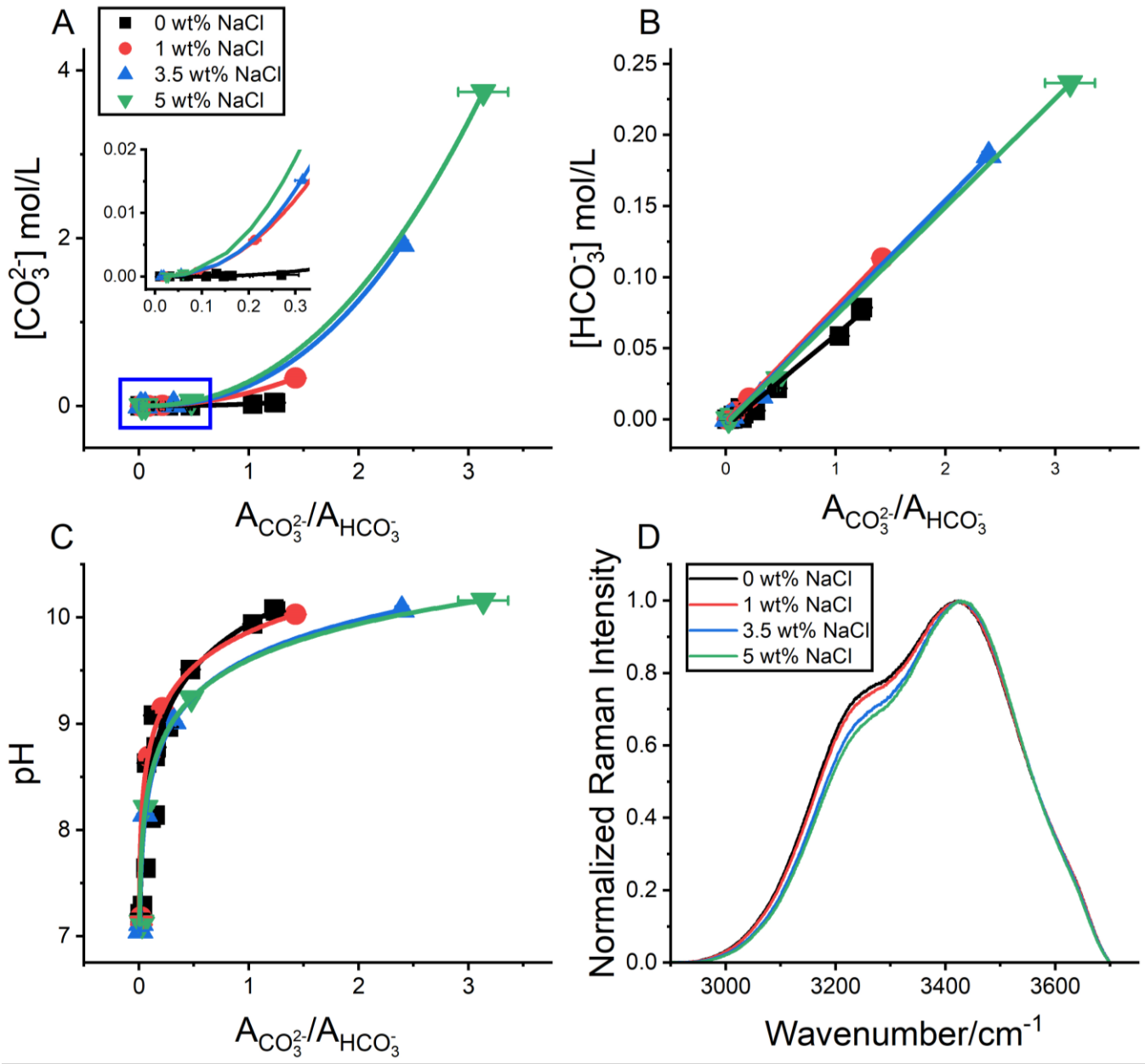

Figure 4. Comparisons of carbonate species concentrations (CO_3^{2-} and HCO_3^-) and pH solution calibrations at various NaCl concentrations (salinities). Solution calibrations of [CO_3^{2-}] (A), [HCO_3^-] (B), and pH (C) versus area ratios between the CO_3^{2-} and HCO_3^- peaks. Normalized Raman OH^- stretch at different NaCl concentrations. Blue box represents the inset within (A). Concentrations are in mol/L.

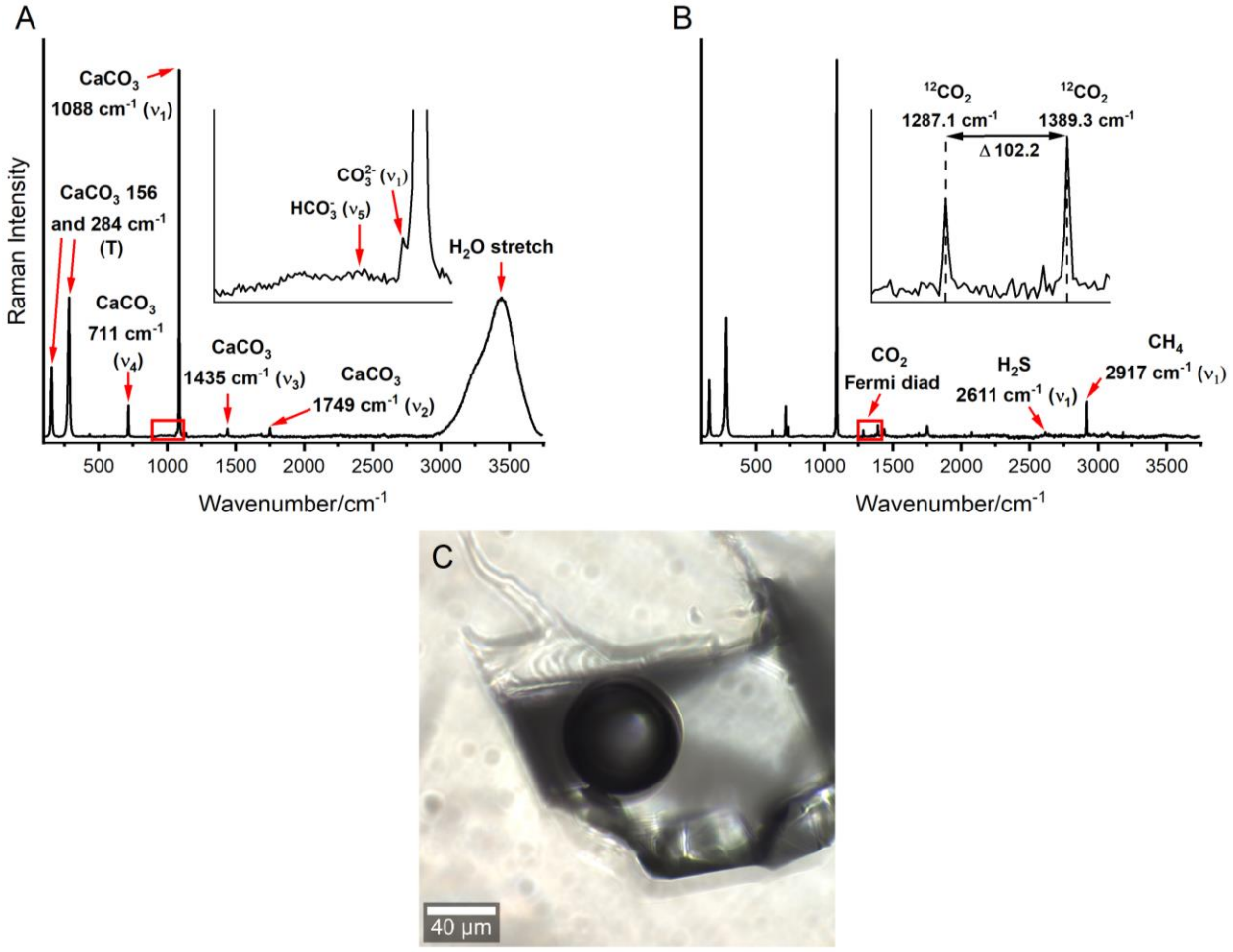

Figure 5. Example Raman spectra of the liquid (A) and gas phase (B) of the large fluid inclusion measured in this study. Liquid phase showing HCO_3^- (1017 cm^{-1}), CO_3^{2-} (1066 cm^{-1}), and H_2O (1630 and 2750-3750 cm^{-1}) peaks with an inset of the red box for the HCO_3^- and CO_3^{2-} peaks. Gas phase shows the CO_2 Fermi diad (1285 and 1388 cm^{-1}), hydrogen sulfide (2611 cm^{-1}), and methane (2917 cm^{-1}). Gas phase inset of the red box shows the CO_2 Fermi diad and the difference between peak distance (Δ) estimates fluid density. Host mineral calcite peaks are present in both in liquid and gas phase spectra at (156, 284, 711, 1088, and 1435 cm^{-1}). Photomicrograph of the analyzed fluid inclusion in Iceland Spar (C). Abbreviations: T, translational lattice; ν_1, symmetric stretching vibration; ν_2, out-of-plane bending vibration; ν_3, antisymmetric stretching vibration; ν_4, in-plane bending vibration.

Table 1. Range of carbonate and bicarbonate concentrations (mol/L), and pH in natural waters.

Environment	$[CO_3^{2-}]$	$[HCO_3^-]$	pH	Reference
Oceans	0.0002 - 0.0003	0.002 - 0.03	7.4 - 8.3	[35,46–48]
Rivers	3.6x10^-8	0.0005 - 0.002	5.28 - 8.5	[35,47,50,69]
Groundwater	0.00169	0.0001 - 0.003	5.1 – 10.7	[51,52,69]
Soil	-	0.0001 - 0.003	4.8 - 10.02	[51,52]
Fluid Inclusions	-	0.007 - 0.014	-	[49]

Table 2. Solutions and associated area ratio of carbonate species to water, with and without the calcite cover slip, measured using Confocal Raman spectroscopy.

NaCl wt%	pH	$[CO_3^{2-}]$	$[HCO_3^-]$	$ACO_3^{2-}/AHCO_3^-$ (non-calcite cover slip)	$ACO_3^{2-}/AHCO_3^-$ (calcite cover slip)
0	10.08	0.0426	0.0762	1.228	-
0	10.06	0.0381	0.0787	1.246	1.259
0	9.94	0.0220	0.0587	1.035	1.047
0	9.51	0.0030	0.0218	0.467	0.456
0	9.08	4.2E-04	0.0080	0.131	-
0	8.97	2.5E-04	0.0062	0.270	0.149
0	8.78	1.1E-04	0.0040	0.159	0.160
0	8.69	7.3E-05	0.0034	0.147	0.151
0	8.63	5.3E-05	0.0029	0.071	-
0	8.14	5.6E-06	0.0009	0.146	0.123
0	8.11	4.8E-06	0.0009	0.110	-
0	7.64	5.5E-07	0.0003	0.063	-
0	7.29	1.1E-07	1.3E-04	0.031	-
0	7.21	7.6E-08	1.1E-04	0.010	-
0	7.18	6.7E-08	1.0E-04	0.025	-
1	10.03	0.3326	0.1133	1.425	-
1	9.15	0.0058	0.0149	0.213	-
1	8.69	0.0007	0.0052	0.090	-
1	7.18	6.6E-07	1.6E-04	0.019	-
1	7.11	4.8E-07	1.4E-04	0.022	-
3.5	10.07	1.927	0.1856	2.393	-
3.5	9.02	0.0152	0.0165	0.315	-
3.5	8.15	2.8E-04	2.2E-03	0.055	-
3.5	7.12	2.4E-06	2.1E-04	0.018	-
3.5	7.05	1.7E-06	1.8E-04	0.013	-
5	10.16	3.7454	0.2365	3.134	-
5	9.24	0.0538	0.0284	0.477	-
5	8.21	4.8E-04	0.0027	0.060	-
5	7.13	3.2E-06	2.2E-04	0.023	-
5	7.11	2.9E-06	2.1E-04	0.028	-

Table 3. Results of $[CO_3^{2-}]$, $[HCO_3^-]$, and pH estimation correlations with and without the calcite cover slip.

	Test	Equation	R^2	95% CI	RMSE
Non-calcite cover slip	$[CO_3^{2-}]$	$y = 0.021x^{3.12}$	0.99	0.018-0.023	0.0013
	$[HCO_3^-]$	$y = 0.064x - 0.004$	0.99	0.059-0.069	0.0035
	pH	$y = \frac{\ln\left(\frac{x}{8.44*10^{-8}}\right)}{1.64}$	0.99	1.42-1.86	0.31
Calcite cover slip	$[CO_3^{2-}]$	$y = 0.020x^{2.83}$	0.99	0.019-0.021	0.0005
	$[HCO_3^-]$	$y = 0.065x - 0.006$	0.99	0.060-0.070	0.002
	pH	$y = \frac{\ln\left(\frac{x}{1.28*10^{-8}}\right)}{1.83}$	0.99	1.48-2.18	0.15

Table 4. Results of $[CO_3^{2-}]$, $[HCO_3^-]$, and pH estimation correlations at different NaCl wt%.

Test	NaCl wt%	Equation	R^2	95% CI	RMSE
$[CO_3^{2-}]$	1 wt%	$y = 0.16x^{2.14}$	0.99	0.15-0.16	0.0021
	3.5 wt%	$y = 0.24x^{2.39}$	0.99	0.24-0.24	0.0055
	5 wt%	$y = 0.24x^{2.39}$	0.99	0.24-0.24	0.020
$[HCO_3^-]$	1 wt%	$y = 0.081x - 0.002$	0.99	0.08-0.082	0.00044
	3.5 wt%	$y = 0.079x - 0.003$	0.99	0.073-0.084	0.0035
	5 wt%	$y = 0.077x - 0.004$	0.99	0.073-0.080	0.0031
pH	1 wt%	$y = \frac{\ln(\frac{x}{7.80 * 10^{-10}})}{2.13}$	0.99	1.9-2.3	0.27
	3.5 wt%	$y = \frac{\ln(\frac{x}{8.26 * 10^{-9}})}{1.93}$	0.99	1.9-2.0	0.025
	5 wt%	$y = \frac{\ln(\frac{x}{3.08 * 10^{-9}})}{2.04}$	0.99	1.93-2.16	0.055

Table 5. Estimated CO_3^{2-} and HCO_3^- concentrations, pH, pCO_2, and CO_2 (ppm) of the calcite fluid inclusion.

$[CO_3^{2-}]$	**$[HCO_3^-]$**	**pH**	**pCO_2**	**CO_2 (ppm)**
0.05 ± 0.08	0.04 ± 0.02	9.46 ± 0.31	-3.62 ± 0.19	240 ± 132